ADVANCED MATERIALS

DOI: 10.1002/adma.200601300

$La(OH)_3$ and La_2O_3 Nanobelts—Synthesis and Physical Properties**

By *Chenguo Hu*, *Hong Liu*, *Wenting Dong*, *Yiyi Zhang*, *Gang Bao*, *Changshi Lao*, and *Zhong L. Wang**

Since the discovery of nanobelts of semiconducting oxides in 2001,[1] planar structures of nanobelts have been intensively researched because they present a good system for examining dimensionally confined and structurally well-defined physical and chemical phenomena.[1,2] Nanobelts, with a rectangular cross section and well-defined faceted surfaces, enable the observation of unique optical-confinement, microcavity, catalysis, and piezoelectricity effects.[3–9] According to classical waveguide theory, waveguides of different cross sections will exhibit different transverse optical modes.[10] Nanobelts with rectangular cross sections have been used as effective Fabry–Perot microcavities for lasing.[11] In the past few years, field-effect transistors,[12] nanometer-sized ultrasensitive gas sensors,[13] resonators,[14] and cantilevers[15] have been fabricated based on individual nanobelts. Thermal transport along the nanobelt has also been measured.[16]

Recent studies on the preparation of rare-earth hydroxide and oxide nanostructures have shown that 1D nanostructures can be prepared by a hydrothermal method, which leads us to believe that 1D nanostructured hydroxides might be prepared via hydrothermal treatment of their counterpart oxides in an autoclave.[17–19] In turn, 1D nanostructured oxides might be obtained from dehydration of their counterpart nanostructured hydroxides.[17,18] However, the high pressure in an autoclave suggests high vessel costs, which, on a large scale, would result in expensive, high-tech production. Here, we develop an approach for the synthesis of ultralong nanobelt-like hydroxides by using a composite-hydroxide-mediated (CHM) synthesis method,[20,21] the advantages of which include simplicity, ease of scale-up, and low costs. The results demonstrate that the CHM approach can not only synthesize complex oxide nanostructures, but can also produce hydroxide nanostructures under normal atmospheric pressure. In this paper, we report the direct growth, by the CHM method, of $La(OH)_3$ nanobelts with typical widths of 30 to 200 nm, thicknesses of 5–30 nm, and lengths of up to a few millimeters. Transmission electron microscopy (TEM), high-resolution TEM (HRTEM), and electron diffraction measurements indicate that the $La(OH)_3$ nanobelts are single-crystalline with a [110] growth direction. La_2O_3 nanobelts with a [010] growth direction were obtained by calcinating $La(OH)_3$ nanobelts in air. The transport properties of a single $La(OH)_3$ nanobelt were measured, and the photoluminescence (PL) characteristics of both $La(OH)_3$ and La_2O_3 nanobelts were investigated.

Lanthanum hydroxide ($La(OH)_3$) nanobelts were prepared by adding $La(CH_3COO)_3$ to a mixture of hydroxides (NaOH/KOH = 51.5:48.5) in a covered Teflon vessel and heating the mixture in a furnace at 200 °C for 48 h. An X-ray diffraction (XRD) pattern of the obtained $La(OH)_3$ product is shown in Figure 1b. All peaks can be perfectly indexed as the pure hexagonal phase ($P6_3/m$ (176), Joint Comittee on Powder Diffraction Standards (JCPDS) file number 36-1481) of $La(OH)_3$, with lattice constants $a = 6.529$ Å and $c = 3.859$ Å.

The morphology of the obtained $La(OH)_3$ product was characterized by scanning electron microscopy (SEM). Figure 1a gives the low-magnification image of $La(OH)_3$, in which the nanobelts are seen to be up to a few millimeters in length. The beltlike structure is seen in the high-magnification images in Figure 1c and d, with typical widths of 30 to 200 nm and thicknesses in the range of 5–30 nm. Energy dispersive X-ray spectroscopy (EDS) analysis, shown in the inset of Figure 1c and d, reveals the presence of La and O with an atomic ratio close to 1:3 (H cannot be detected by EDS). By examining the nanobelts in detail, we found that the ends have an arrowlike shape (Fig. 1e) and that the cross sections are rectangular (Fig. 1f).

[*] Prof. Z. L. Wang, Prof. C. G. Hu, Prof. H. Liu, C. S. Lao
School of Materials Science and Engineering
Georgia Institute of Technology
Atlanta, GA 30332–0245 (USA)
E-mail: zhong.wang@mse.gatech.edu
Prof. C. G. Hu
Department of Applied Physics, Chongqing University
Chongqing 400044 (P.R. China)
Prof. H. Liu
State Key Laboratory of Crystal Materials, Shandong University
Jinan 250100 (P.R. China)
Dr. W. T. Dong
School of Chemistry & Biochemistry
Georgia Institute of Technology
Atlanta, GA 30332-0245 (USA)
Dr. Y. Y. Zhang, Prof. G. Bao
Department of Biomedical Engineering
Georgia Institute of Technology and Emory University
Atlanta, GA 30332-0245 (USA)

[**] The research was supported by an NSF grant DMR-9733160, the NASA Vehicle Systems Program and Department of Defense Research and Engineering (DDR&E), the Defense Advanced Research Projects Agency (Award No. N66001-04-1-8903), and the CCNE from the NIH. C.G.H. and H.L. are grateful for the support of the NSFC (No. 60376032, 90406024, and 50572052). G.B. is grateful for the support of the NIH (1U01HL80711-01).

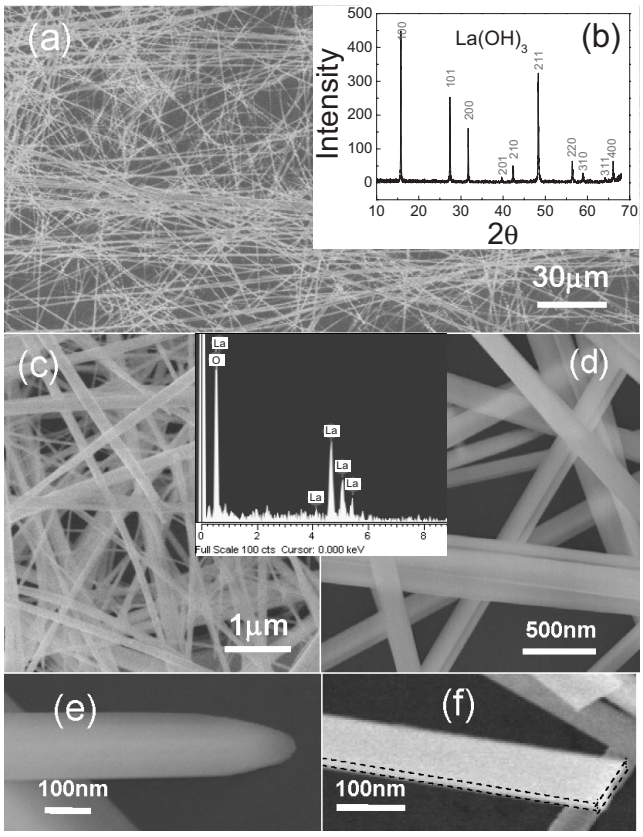

Figure 1. a) Low-magnification SEM image of the $La(OH)_3$ products, indicating lengths of up to several millimeters. b) A typical XRD pattern of the as-synthesized $La(OH)_3$ product. c,d) High-magnification SEM images of the $La(OH)_3$ product, indicating the nanobelts width of tens to more than one hundred nanometers. Inset: Energy dispersive X-ray spectroscopy (EDS) analysis of the nanobelts, showing the presence of La and O (H cannot be detected by EDS). e,f) An arrow-shaped end (e) and cross section (f) of a nanobelt, exhibiting a thickness of 10 nm.

The nanobelt structure of $La(OH)_3$ was further examined by TEM and HRTEM. Figure 2a shows a typical low-magnification TEM image of the $La(OH)_3$ nanobelts. The selected-area electron diffraction (SAED) pattern (Fig. 2c), taken from the nanobelt in Figure 2b, can be indexed as a hexagonal $La(OH)_3$ single crystal with a [110] growth direction. Figure 2d gives the HRTEM image of a single-crystalline nanobelt.

The following possible growth mechanism for the $La(OH)_3$ nanobelts in hydroxide solution is suggested: Although the melting points (T_m) of both pure sodium hydroxide and potassium hydroxide are over 300 °C (T_m(NaOH) = 323 °C, T_m(KOH) = 360 °C), the eutectic point for the composition NaOH/KOH = 51.5:48.5 is only about 165 °C. During the reaction process, the hydroxides not only play a role as solvents for lowering the reaction temperature but also act as reactants. In the molten hydroxide, $La(CH_3COO)_3$ reacts with NaOH/KOH to produce crystalline $La(OH)_3$ nuclei, which then grow along the [110] direction to form nanobelts. The simple chemical reaction (where M denotes Na or K) is as follows:

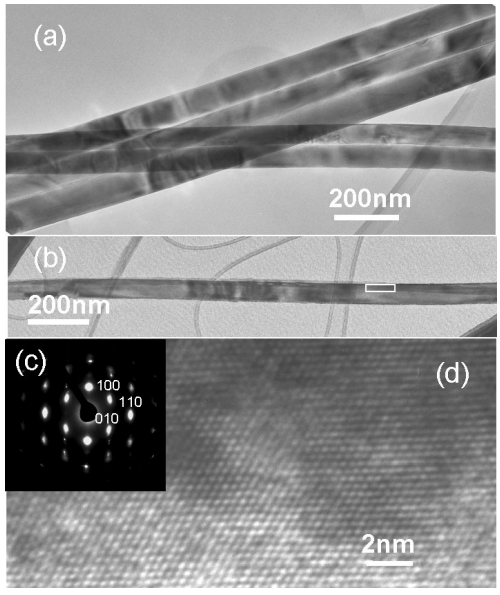

Figure 2. a) TEM image of the $La(OH)_3$ nanobelts. b) TEM image of a single $La(OH)_3$ nanobelt. c) Electron diffraction pattern and d) HRTEM image of the selected area in (b), indicating that the nanobelt is single-crystalline with a growth direction of [110].

$$La(CH_3COO)_3 + 3\,MOH \rightarrow La(OH)_3 + 3\,M(CH_3COO) \qquad (1)$$

Because of the large viscosity of the hydroxide, the formation of $La(OH)_3$ nanostructures is slow, and it is not easy for the nanostructures to agglomerate. This is the key to obtaining disperse single-crystalline nanostructures from the reaction without using a surface-capping material. This growth mechanism is quite different from the previously mentioned synthesis methods,[17–19] in which the oxides dissolve and the hydroxides form under hydrothermal treatment in an autoclave, subsequently recrystallizing and growing into nanostructures through a dissolution–recrystallization process.

Although several reports have presented the synthesis of 1D rare-earth nanometer-sized hydroxides,[17–19] no further studies on the properties of such nanostructures were described in these reports. We fabricated a pair of electrodes for connecting a single $La(OH)_3$ nanobelt to characterize its electrical transport properties. The device was prepared by ac electrophoresis, and the contacts were improved through local deposition of Pt by focused-ion-beam (FIB) microscopy.[22] The current (I) increased linearly with the voltage (V), as shown in the I–V diagram (Fig. 3a), which indicates Ohmic behavior. The resistivity of the nanobelt was calculated as 1.7 $k\Omega\,nm^{-1}$. Figure 3b shows an SEM image of the single-nanobelt device. The detectable conductive behavior of a single nanobelt presented here promises the potential application of $La(OH)_3$ nanobelts in sensors by designing a corresponding electronic device.

When the $La(OH)_3$ nanobelts were calcined in air at 690 °C for 6 h, La_2O_3 nanobelts were obtained. Figure 4a shows an XRD pattern of pure La_2O_3; all peaks can be indexed as the

ADVANCED MATERIALS

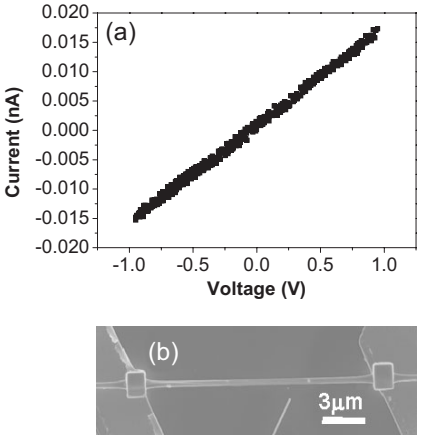

Figure 3. a) Current–voltage (*I*–*V*) diagram of a single nanobelt, showing the constant resistivity. b) SEM image of the single nanobelt electrode.

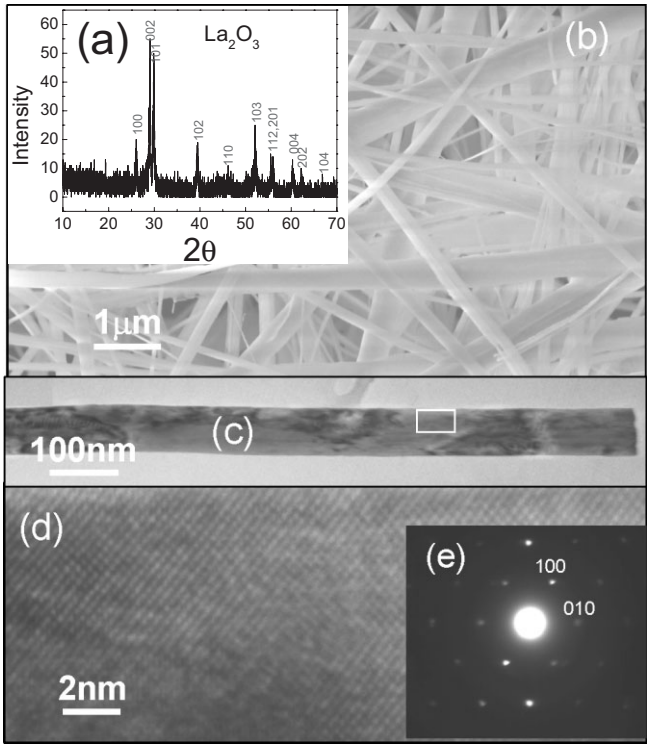

Figure 4. a) XRD pattern of the La_2O_3 nanobelts. b) SEM image of La_2O_3 nanobelts. The La_2O_3 product was obtained by calcination of the as-synthesized $La(OH)_3$ nanobelts at 690 °C for 6 h in air. c) A typical TEM image of a single La_2O_3 nanobelt. d) HRTEM image of the selected area in (c). e) Electron diffraction pattern, indicating the nanobelt is single-crystalline.

pure hexagonal phase ($P\bar{3}m1$ (164), JCPDS file number 05-0602) of La_2O_3 with lattice constants $a = 3.397$ Å and $c = 6.129$ Å. The unit-cell size of the La_2O_3 nanobelts is smaller than that of the $La(OH)_3$ nanobelts. The morphology of La_2O_3 nanobelts is shown in Figure 4b, where it is seen that the La_2O_3 nanobelts retain the original beltlike shape after calcination. Figure 4c shows a low-magnification TEM image of a typical La_2O_3 nanobelt. The HRTEM image and SAED pattern in Figure 4d and e, respectively, indicate a hexagonal single-crystal phase of La_2O_3 with a [010] growth direction.

To explore the possibilities of fluorescence labeling by $La(OH)_3$ and La_2O_3 nanobelts, we carried out fluorescence imaging and PL measurements at room temperature. Figure 5a and b shows a bright-field and fluorescence image, respectively, for a bundle of $La(OH)_3$ nanobelts under UV excitation. As in the bright-field image, the nanobelts can be clearly distinguished in the fluorescence image in Figure 5b, indicating their potential use in biological labeling. Detailed PL properties of the nanobelts are given by the PL excitation and emission spectra in Figure 5c and d, respectively. The PL experiments were conducted by making uniform thin films of the $La(OH)_3$ and La_2O_3 nanobelts on Si wafers. Figure 5c shows the excitation spectrum of the $La(OH)_3$ nanobelts at a controlled emission wavelength of 490 nm, indicating absorption around 353 nm. At an excitation wavelength of 353 nm, PL emission appears at a wavelength of ca. 410 nm, as shown in Figure 5d, indicating the lower radiative photon energy compared to the absorption photon energy. Similar PL spectra are detected for the La_2O_3 nanobelts, with an absorption wavelength of ca. 363 nm (at a controlled emission wavelength of 519 nm) and an emission wavelength of ca. 416 nm (at an excitation wavelength of 360 nm), as shown in Figure 5e and f, respectively. The emission spectra of the $La(OH)_3$ and La_2O_3 nanobelts indicate that they can emit purple light.

Based on the luminescence theory of rare-earth atoms,[23] La^{III} does not radiate any luminescence because there are zero electrons in the 4f shell, and thus only one possibly optical state: $^1S_0$. Therefore, La cannot be regarded as an emission center and cannot radiate light from the inner atomic 4f shell when crystalline $La(OH)_3$ and La_2O_3 are formed. To further examine if the emission originates from a transition between the conduction and valence band, we have calculated the bandgap (E_g) of a La_2O_3 crystal agreeing with the XRD data of our experiment ($P\bar{3}m1$ (164), JCPDS 05-0602, $a = 3.397$ Å, $c = 6.129$ Å) by using the CASTEP software package, based on first-principles pseudopotential calculation. The E_g value of La_2O_3 was calculated as 3.8 eV. However, the absorption energy of the La_2O_3 nanobelts is around 3.42 eV (363 nm) in Figure 5e, which is lower than the E_g value of 3.8 eV. Therefore, the emission of 416 nm could not contribute to the transition from the conduction band to the valence band, because the energy gap of 3.8 eV corresponds to the photoabsorption of 327 nm, which does not appear in the excitation spectrum (Fig. 5e).

We propose that the emission at 416 nm comes from a deep-level or trap-state emission, as there is an energy loss of 0.91 eV. The emission transition has been attributed to singly ionized oxygen vacancies in La_2O_3, and the emission results from the radiative recombination of a photogenerated hole with an electron occupying an oxygen vacancy, which is commonly referred to as the green luminescence mechanism of a

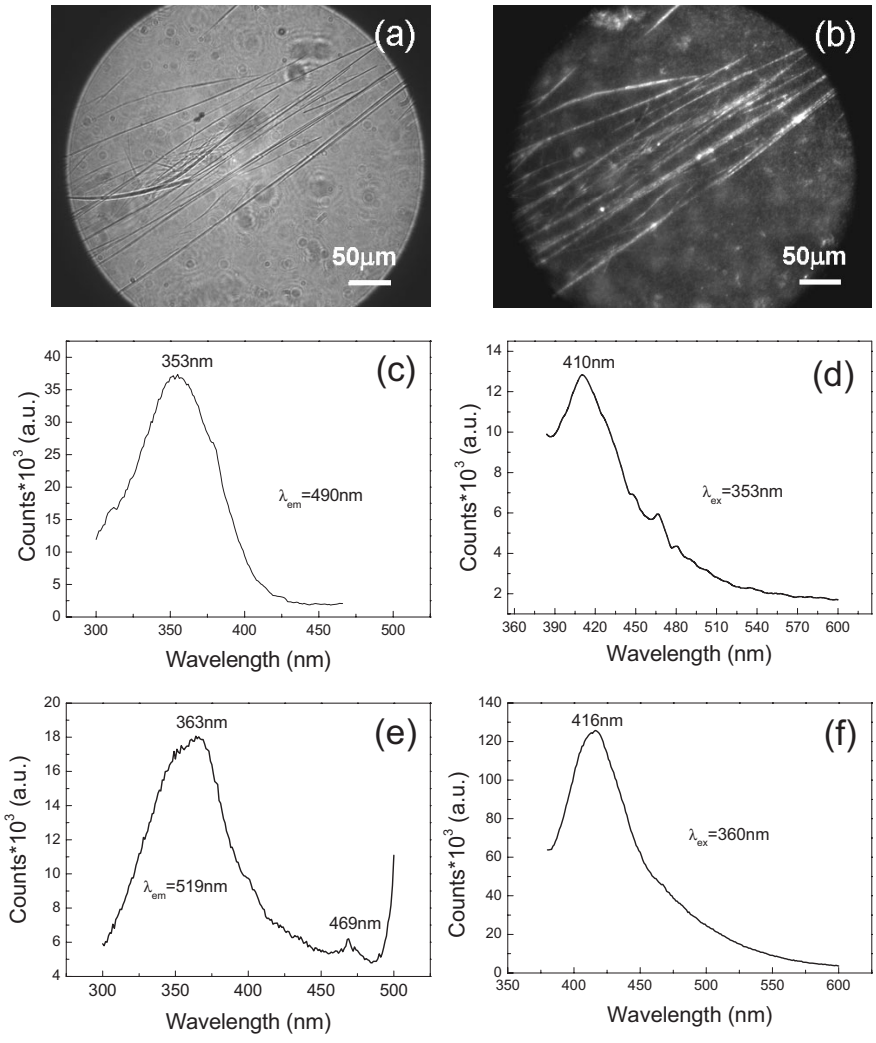

Figure 5. a,b) Bright-field (a) and fluorescence (b) images of a bundle of $La(OH)_3$ nanobelts under UV excitation. c) PL excitation spectrum of $La(OH)_3$ nanobelts with a controlled emission wavelength of 490 nm. d) PL emission spectrum of $La(OH)_3$ at an excitation wavelength of 353 nm. e) PL excitation spectrum of La_2O_3 with a controlled emission wavelength of 519 nm. f) PL emission spectrum of La_2O_3 at an excitation wavelength of 360 nm.

ZnO nanostructure.[24,25] The morphology of the nanobelts, with a high surface-to-volume ratio, also plays a major role in the density of singly ionized oxygen vacancies and the charge state of this defect, due to the existence of surface depletion, and thus in controlling the emission intensity.[24,25]

Lanthanum hydroxide has many potential applications.[19] The surface hydroxyl groups may act as active sites for possible surface-modification treatment through condensation reactions with amino acids or biologically active molecules, and, thus, lanthanum hydroxide nanobelts may have potential in the field of biological labeling. In addition, the similarity of the crystal structure and lattice constants suggests that doped lanthanum hydroxide nanobelts could be prepared by a similar growth process, as lattice mismatching would not be a serious concern. Meanwhile, because hydroxides can be easily converted into oxides or sulfides (through sulfuration), $La(OH)_3$ or co-doped $La(OH)_3$ nanobelts can act as important precursor to lanthanum oxide or lanthanum sulfide nanobelts.

In summary, we have developed a facile composite-hydroxide-mediated synthesis method to prepare ultralong $La(OH)_3$ nanobelts. The detectable conductive behavior of a single nanobelt promises the potential application of the $La(OH)_3$ nanobelts in sensors, by designing the corresponding electronic devices. The La_2O_3 nanobelts can be obtained by calcinations of $La(OH)_3$ nanobelts. Both the $La(OH)_3$ and La_2O_3 nanobelts can fluoresce with purple light under UV excitation, which may be useful for biological labeling.

Experimental

To prepare $La(OH)_3$ nanobelts, 0.1 g of $La(CH_3COO)_3$, to which 1 mL deionized water was added, was put into 18 g of mixed hydroxides (NaOH/KOH = 51.5:48.5) in a covered Teflon vessel and heated at 200 °C for 48 h in a furnace. When the vessel had cooled to room temperature, the solid product was washed by using deionized water and filtered. The product was then washed with diluted HCl (pH 1.2) to remove other hydroxides. Clean $La(OH)_3$ nanobelts were obtained after washing twice with deionized water. To obtain the La_2O_3, calcination attempts of the $La(OH)_3$ nanobelts were carried out from 300 to 700 °C. The pure La_2O_3 nanobelts could be successfully obtained by calcining the $La(OH)_3$ nanobelts at 690 °C for 6 h in air.

Field-emission scanning electron microscopy (LEO 1530) and transmission electron microscopy (JEOL 100C) were used to characterize the morphology and size of the as-synthesized samples. A Philips X-ray diffractometer and energy-dispersive X-ray spectroscopy (EDS) were used to investigate the chemical composition. The structure of the $La(OH)_3$ nanobelts was characterized using HRTEM (Hitachi HF-2000). The fabrication of a single $La(OH)_3$ nanobelt based device was carried out by ac electrophoresis [22]. We used an Axiovert S100 fluorescent microscope (Zeiss) equipped with a 100 W mercury lamp. PL experiments were measured on a SPEX Fluorolog-2 spectrofluorometer by making uniform thin films of the $La(OH)_3$ and La_2O_3 nanobelts on Si wafers. All experiments were performed at room temperature.

Received: June 13, 2006
Revised: August 31, 2006
Published online: January 16, 2007

[1] Z. W. Pan, Z. R. Dai, Z. L. Wang, *Science* **2001**, *291*, 1947.
[2] W. Shi, H. Peng, N. Wang, C. P. Li, L. Xu, C. S. Lee, R. Kalish, S.-T. Lee, *J. Am. Chem. Soc.* **2001**, *123*, 11 095.
[3] M. S. Hu, W. M. Wang, T. T. Chen, L. S. Hong, C. W. Chen, C. C. Chen, Y. F. Chen, K. H. Chen, L. C. Chen, *Adv. Funct. Mater.* **2006**, *16*, 537.

[4] J. L. Zhang, J. M. Du, B. X. Han, Z. M. Liu, T. Jiang, Z. F. Zhang, *Angew. Chem. Int. Ed.* **2006**, *45*, 1116.
[5] J. Zhang, Y. D. Yang, F. H. Jiang, B. L. Xu, J. P. Li, X. C. Wang, S. M. Wang, *Nanotechnology* **2005**, *16*, 2887.
[6] J. C. Johnson, H. J. Choi, K. R. Knutsen, R. D. Schaller, P. Yang, R. J. Saykally, *Nat. Mater.* **2002**, *1*, 106.
[7] M. Huang, S. Mao, H. Feick, H. Yan, Y. Wu, H. Kind, E. Weber, R. Russo, P. Yang, *Science* **2001**, *292*, 1897.
[8] Z. L. Wang, *J. Phys. Condens. Matter* **2004**, *16*, R829.
[9] J. H. Song, X. D. Wang, E. Riedo, Z. L. Wang, *Nano Lett.* **2005**, *5*, 1954.
[10] *Fundamentals of Optical Waveguides* (Ed: K. Okamoto), Academic, San Diego, CA **2000**.
[11] H. Yan, J. Johnson, M. Law, R. He, K. Knutsen, J. R. McKinney, J. Pham, R. Saykally, P. Yang, *Adv. Mater.* **2003**, *15*, 1907.
[12] M. S. Arnold, P. Avouris, Z. L. Wang, *J. Phys. Chem. B* **2003**, *107*, 659.
[13] E. Comini, G. Faglia, G. Sberveglieri, Z. W. Pan, Z. L. Wang, *Appl. Phys. Lett.* **2002**, *81*, 1869.
[14] X. D. Bai, P. X. Gao, Z. L. Wang, E. G. Wang, *Appl. Phys. Lett.* **2003**, *82*, 4806.
[15] W. Hughes, Z. L. Wang, *Appl. Phys. Lett.* **2003**, *82*, 2886.
[16] L. Shi, Q. Hao, C. Yu, D. Kim, N. Mingo, X. Y. Kong, Z. L. Wang, *Appl. Phys. Lett.* **2004**, *84*, 2638.
[17] A. W. Xu, Y. P. Fang, L. P. You, H. Q. Liu, *J. Am. Chem. Soc.* **2003**, *125*, 1494.
[18] Y. P. Fang, A. W. Xu, L. P. You, R. Q. Song, J. C. Yu, H. X. Zhang, Q. Li, H. Q. Liu, *Adv. Funct. Mater.* **2003**, *13*, 955.
[19] X. Wang, Y. D. Li, *Angew. Chem. Int. Ed.* **2002**, *41*, 4790.
[20] H. Liu, C. G. Hu, Z. L. Wang, *Nano Lett.* **2006**, *6*, 1535.
[21] C. G. Hu, H. Liu, C. S. Lao, L. Y. Zhang, D. Davidovic, Z. L. Wang, *J. Phys. Chem. B* **2006**, *110*, 14 050.
[22] C. S. Lao, J. Liu, P. X. Gao, L. Y. Zhang, D. Davidovic, R. Tummala, Z. L. Wang, *Nano Lett.* **2006**, *6*, 263.
[23] J. Y. Li, *Luminescent Materials of Rare Earths and Their Applications*, Chemical Industry, Beijing **2003**, p. 8.
[24] K. Vanheusden, W. L. Warren, C. H. Seager, D. R. Tallant, J. A. Voigt, B. E. Gnade, *J. Appl. Phys.* **1996**, *79*, 7983.
[25] M. H. Huang, Y. Y. Wu, H. Feick, N. Tran, E. Weber, P. D. Yang, *Adv. Mater.* **2001**, *13*, 113.

